Neuron
Article

Functional Architecture of an Optic Flow-Responsive Area that Drives Horizontal Eye Movements in Zebrafish

Fumi Kubo,[1] Bastian Hablitzel,[2] Marco Dal Maschio,[1] Wolfgang Driever,[2] Herwig Baier,[1,*] and Aristides B. Arrenberg[2]
[1]Max Planck Institute of Neurobiology, Department Genes - Circuits - Behavior, Am Klopferspitz 18, D-82152 Martinsried, Germany
[2]Developmental Biology, Institute Biology 1, Faculty of Biology, and Center for Biological Signaling Studies (BIOSS), University of Freiburg, Hauptstrasse 1, D-79104 Freiburg, Germany
*Correspondence: hbaier@neuro.mpg.de
http://dx.doi.org/10.1016/j.neuron.2014.02.043

SUMMARY

Animals respond to whole-field visual motion with compensatory eye and body movements in order to stabilize both their gaze and position with respect to their surroundings. In zebrafish, rotational stimuli need to be distinguished from translational stimuli to drive the optokinetic and the optomotor responses, respectively. Here, we systematically characterize the neural circuits responsible for these operations using a combination of optogenetic manipulation and in vivo calcium imaging during optic flow stimulation. By recording the activity of thousands of neurons within the area pretectalis (APT), we find four bilateral pairs of clusters that process horizontal whole-field motion and functionally classify eleven prominent neuron types with highly selective response profiles. APT neurons are prevalently direction selective, either monocularly or binocularly driven, and hierarchically organized to distinguish between rotational and translational optic flow. Our data predict a wiring diagram of a neural circuit tailored to drive behavior that compensates for self-motion.

INTRODUCTION

Animals rely on optic flow signals generated by the movement of their bodies relative to the visual surroundings to orient and navigate within their environment. Frequently, to compensate for perceived self-motion, they employ stabilization behaviors. Two prominent examples of such behavior in zebrafish are the optokinetic response (OKR), a behavior in which the eyes move to hold the gaze steady (Brockerhoff et al., 1995; Huang and Neuhauss, 2008), and the optomotor response (OMR), by which the animals actively swim to stabilize their position with respect to a drifting visual background (Neuhauss et al., 1999; Orger et al., 2000).

The perception of optic flow, which underlies the OKR and OMR, is mediated by direction-selective (DS) cells, which are characterized by their asymmetrical responses to stimuli moving in different directions. DS cells are found at many levels in the visual system. In the retina, direction selectivity is implemented in retinal ganglion cells (RGCs) (Barlow and Hill, 1963; Nikolaou et al., 2012; Vaney et al., 2012). Within the subcortical areas, DS cells are abundant in the pretectum in the diencephalon and the accessory optic system (AOS). These regions receive direct inputs from RGCs in the contralateral retina, as has been shown in a range of vertebrate species (Scalia, 1972; Montgomery et al., 1981; Vanegas and Ito, 1983; Karten et al., 1977). In teleosts, a single pretectal area (area pretectalis [APT]) encodes the two horizontal (nasalward and temporalward) and two vertical (up and down) motion directions (Klar and Hoffmann, 2002; Masseck and Hoffmann, 2009a, 2009b). Brain nuclei that respond to ipsiversive optic flow (i.e., grating motion toward the side of the brain in which the recording was carried out) include the nucleus of the optic tract (NOT) and the dorsal terminal nucleus (DTN) in mammals and the nucleus lentiformis mesencephali (LM) in amphibians, reptiles, and birds. Lesions of these nuclei abolish the OKR to ipsiversive optic flow (Cazin et al., 1980; Gioanni et al., 1983; Kato et al., 1988; Precht and Strata, 1980; Schiff et al., 1990). Electrical stimulation, on the other hand, elicits an ipsiversive OKR in the absence of visual stimulation (Collewijn, 1975; Schiff et al., 1988). These findings indicated that the ipsiversive responsive cells in the pretectum/AOS mediate the horizontal OKR (Masseck and Hoffmann, 2009b). Neurons that respond to contraversive motion have not been found in the mammalian pretectum/AOS but are present in teleost fish (Masseck and Hoffmann, 2009b).

It is unclear how optic flow information is used to drive OKR and OMR. In lateral-eyed animals, the motion information in the two eyes could be compared to distinguish rotational optic flow from translational optic flow, and this operation would require neurons with binocular receptive fields. Pretectal binocularity could arise by commissural connections within the pretectum itself (Ferrari et al., 2009; Pereira Júnior et al., 1994; Pereira et al., 2000; Reber et al., 1991) or via input from a higher center, like the visual cortex in mammals (Markner and Hoffmann, 1985). Fish have completely crossed optic chiasms, and binocular APT neurons are apparently rare. This has led to the proposal that binocular information is integrated downstream of visual brain areas, in brain structures such as the inferior olive

or the vestibulocerebellum (Masseck and Hoffmann, 2008, 2009a). Whether and how pretectal neurons are involved in the discrimination of rotation from translation is therefore poorly understood.

In zebrafish, the OMR and OKR have widely been used as readouts for visual function in mutagenesis screens (Brockerhoff et al., 1995; Muto et al., 2005; Neuhauss et al., 1999), yet the brain structures mediating these behaviors have not been identified. Intriguingly, fish perform the OKR in response to rotational motion and the OMR mainly in response to translational motion, and thus, rotation and translation are tightly linked with different behavioral output. Here we took advantage of recent advances in optogenetics and functional imaging (Baier and Scott, 2009; Wyart and Del Bene, 2011; Del Bene and Wyart, 2012; McLean and Fetcho, 2011). We first functionally localized the APT using optogenetic gain-of-function and loss-of-function manipulations. Subsequently, we performed in vivo two-photon calcium imaging (Euler et al., 2009; Renninger and Orger, 2013) using the genetically encoded calcium indicator GCaMP5G (Ahrens et al., 2013; Akerboom et al., 2012) in conjunction with rotational and translational optic flow stimuli. The large population size that can be sampled by functional imaging of the small, transparent larval brain enabled us to systematically characterize the response properties of APT neurons. We discovered an array of highly specific response types that had apparently been missed by previous electrophysiological studies in other species. The new classes include cells that process binocular translational or binocular rotational stimuli via excitatory or inhibitory interactions. Neurons with similar response profiles are clustered in overlapping spatial domains within the APT. Our analysis predicts a detailed wiring diagram of the larval zebrafish APT that drives horizontal eye movements.

RESULTS

Optogenetic Perturbations Show that the Pretectum Is Necessary and Sufficient for the OKR

We tested the contribution of the pretectum to the OKR in larval zebrafish by targeted optogenetic stimulation of candidate brain volumes. The *Gal4s1101t* enhancer-trap line was used to drive expression of the light-activatable cation channel channelrhodopsin2 (ChR2) in almost all neurons of the CNS (Arrenberg et al., 2009). Fish larvae (5–6 days postfertilization) were mounted in agarose, with the eyes free to move. An optic fiber was positioned in parallel to the fish's body axis and angled horizontally (Figure 1A). When, in the absence of visual stimulation, a pretectal area in *Gal4s1101t*; *UAS*:*ChR2-mCherry* fish was unilaterally stimulated (488 nm) for 10 s, both eyes performed conjugate movements toward the ipsilateral side of the fiber stimulation, which were followed by a rapid eye movement in the opposite direction, and the eye movements in the alternating directions were repeated during illumination (Figure 1A; Movie S1 available online). We did not observe this effect when a similar volume of tissue was stimulated in the tectum (Figure 1A). The average velocity of the slow phase was strongly dependent on the laser power ($R^2 = 0.9512$), while the amplitude did not show a strong correlation ($R^2 = 0.3412$) (Figures 1B and 1C). The eye velocity of the ChR2-induced, slow-phase eye movements was within the range of that seen during the OKR (~5°/s to 30°/s, depending on the stimulus velocity) (Huang et al., 2006; Qian et al., 2005). Together, the conjugate slow and fast eye movements in opposing directions closely resembled the OKR.

To visualize the pretectal area in which ChR2 stimulation induced OKR-like eye movements, we photoconverted Kaede through the optic fiber (405 nm) in *Gal4s1101t*; *UAS*:*ChR2-mCherry*; *UAS*:*Kaede* triple transgenic fish following ChR2 stimulation. We observed a column of photoconverted cells that included a region in the ventral midbrain/diencephalon below the tectum (Figures 1D–1E). This area roughly corresponded to one of the arborization fields of RGC axons, AF9, as labeled in *Atoh7*:*Gal4*; *UAS*:*Dendra* fish (Figure 1F) (Burrill and Easter, 1994). The photoconverted region did not reach the hindbrain due to the angled orientation of the optic fiber.

We next tested if the pretectal area is necessary for the OKR using a line expressing UAS-linked halorhodopsin in combination with the same Gal4 driver line to silence neural activity in the larval brain (Arrenberg et al., 2009). We presented a moving grating to one eye in order to drive the OKR. As reported previously, monocular presentation of the OKR stimulus evoked yoked movements of both eyes (Qian et al., 2005; Rinner et al., 2005). Upon illumination (633 nm) of the pretectal area contralateral to the stimulated eye (Figure 1G), the slow-phase eye movements of the OKR were bilaterally stalled. Illumination of the tectum in experimental animals or illumination of the pretectum in control animals (*Gal4s1101t*; *UAS*:*Kaede*) did not affect the OKR (Figures 1G and 1H). Our ChR2 and NpHR experiments indicate that the pretectal area is necessary and sufficient for the OKR.

Optic Flow Stimuli Evoke Direction-Selective Responses in the Pretectum

We next asked whether and how the pretectum physiologically responds to whole-field motion. A *HuC*:*GCaMP5G* transgenic line (Ahrens et al., 2013) was used to express the genetically encoded calcium indicator GCaMP5G in the majority of neurons. We systematically imaged the pretectum region at 12–15 equally spaced (5 or 10 μm) dorso-ventral levels spanning about 70 μm in depth and presented gratings that moved in either a clockwise (CW) or counter-clockwise (CCW) direction at different temporal frequencies (Figure 2A). To identify neurons that respond to the visual stimulus in an unbiased manner, we applied the pixel-by-pixel regression-based approach described previously (Miri et al., 2011). This allows a semiautomatic identification of image pixels whose fluorescence time series is correlated with a particular time-varying variable (called regressor). To identify pixels that are responsive to the CW or CCW motion, we used a regressor that equaled 1 during CW motion and −1 during CCW motion (see Experimental Procedures). Furthermore, the regressor was convolved to account for the slow kinetics of the GCaMP5G signal (Figure 2A, DS regressor). Subsequently, regions of interest (ROIs) were drawn manually over contiguous areas of identified pixels that corresponded to the outline of a cell. We refer to these ROIs as "cells" here, although it is possible that a

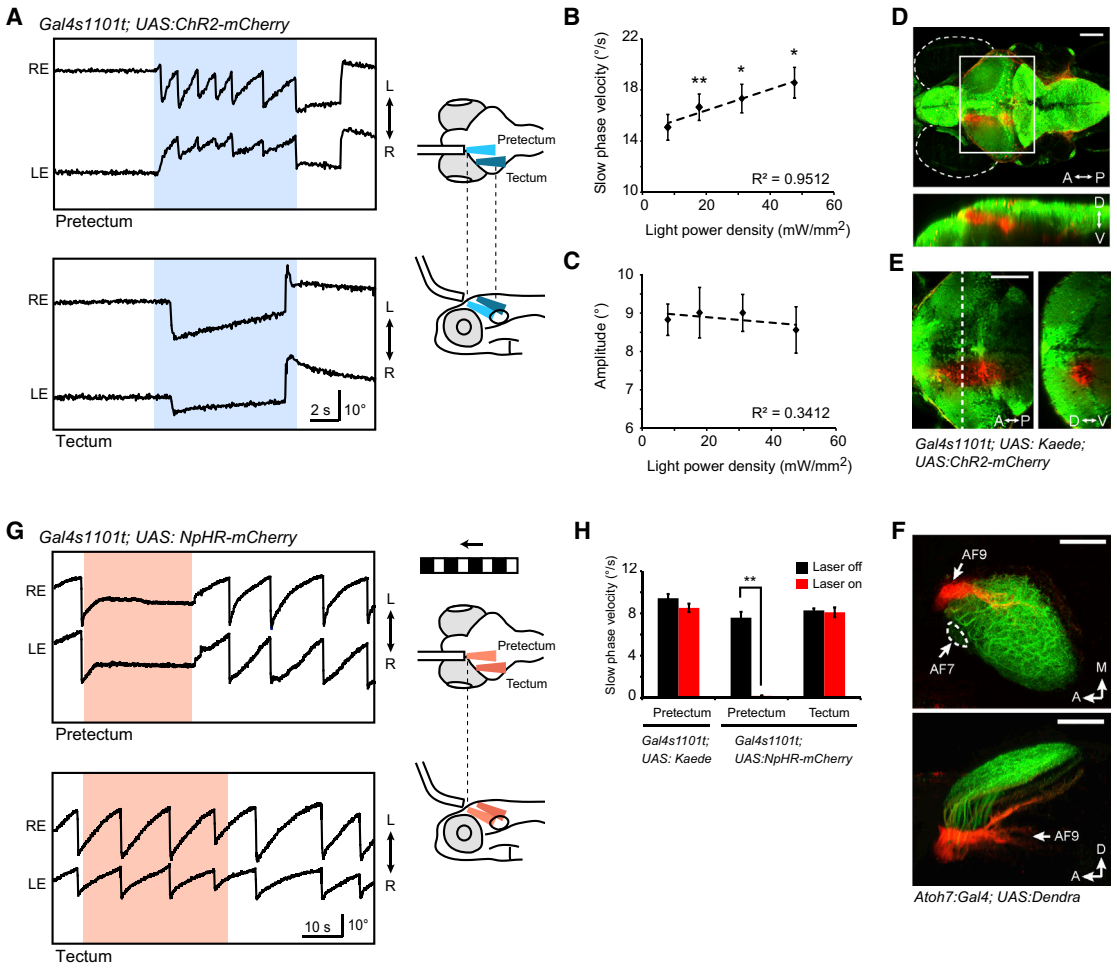

Figure 1. Optogenetic Manipulations of the Pretectal Area during OKR

(A) Angular eye position during ChR2 stimulation in the pretectal (top) and tectal (bottom) area. Blue-shaded regions depict the epoch of ChR2 stimulation (power density = ~18 mW/mm^2). Schematics of optical stimulation are shown on the right. An optic fiber (diameter 50 μm) was positioned in parallel to the fish's longitudinal axis and angled ventrally. For tectum stimulation, the optic fiber was shifted laterally and posteriorly compared to the pretectum stimulation. LE indicates left eye; RE indicates right eye.

(B and C) Velocity and amplitude of slow-phase eye movements evoked by ChR2 stimulation as a function of laser power density. Right and left stimulations were pooled, and the eye contralateral to the stimulated side was measured (n = 6 fish). **p < 0.01; *p < 0.05; paired t test against the lowest laser power density. R^2 indicates square of Pearson's correlation coefficient.

(D) Confocal z projection of a *Gal4s1101t*; *UAS:ChR2-mCherry*; *UAS:Kaede* fish in dorsal view (top) and side view (bottom). Kaede was locally photoconverted (red) in the left pretectum.

(E) Single optical section (3.6 μm) of the photoconverted area; corresponding to the white box in (D) in dorsal view (left). A frontal view at the level of dashed line is shown on the right.

(F) Photoconversion of RGC axons. Confocal z projection of an *Atoh7:Gal4*; *UAS:Dendra* larva after photoconversion using a 50 μm optic fiber in dorsal view (top panel) and side view (bottom panel). Photoconverted Dendra (red) was detected in AF9 and the deepest layer of the tectum (which receives projections from RGCs that project to AF9), whereas AF7 and most of the tectum (AF10) remained unconverted (green).

(G) Representative eye traces of an NpHR-stimulated animal during OKR. Red-shaded regions indicate the epoch of NpHR stimulation (633 nm; ~140 mW/mm^2). Schematics of visual and optical stimulations are shown on the right.

(H) Slow-phase velocity of the OKR under laser off and on conditions (n ≥ 6 fish for each condition). The eye contralateral to the NpHR-stimulated side was measured. **p = 0.00064, paired t test. A indicates anterior; P indicates posterior; D indicates dorsal; V indicates ventral; M indicates medial. Error bars indicate SEM. Scale bars show 100 μm (D–F).

fraction of the ROIs contain signals of neighboring cell somata or neurites (Figure S1). We first imaged calcium responses in an agarose-embedded fish with the eyes free to move during optic flow stimulation, while simultaneously tracking the eye movements. By applying the regression-based method, we successfully found cells correlated with the visual stimulus or with both the visual stimulus and the eye position (Figure S2).

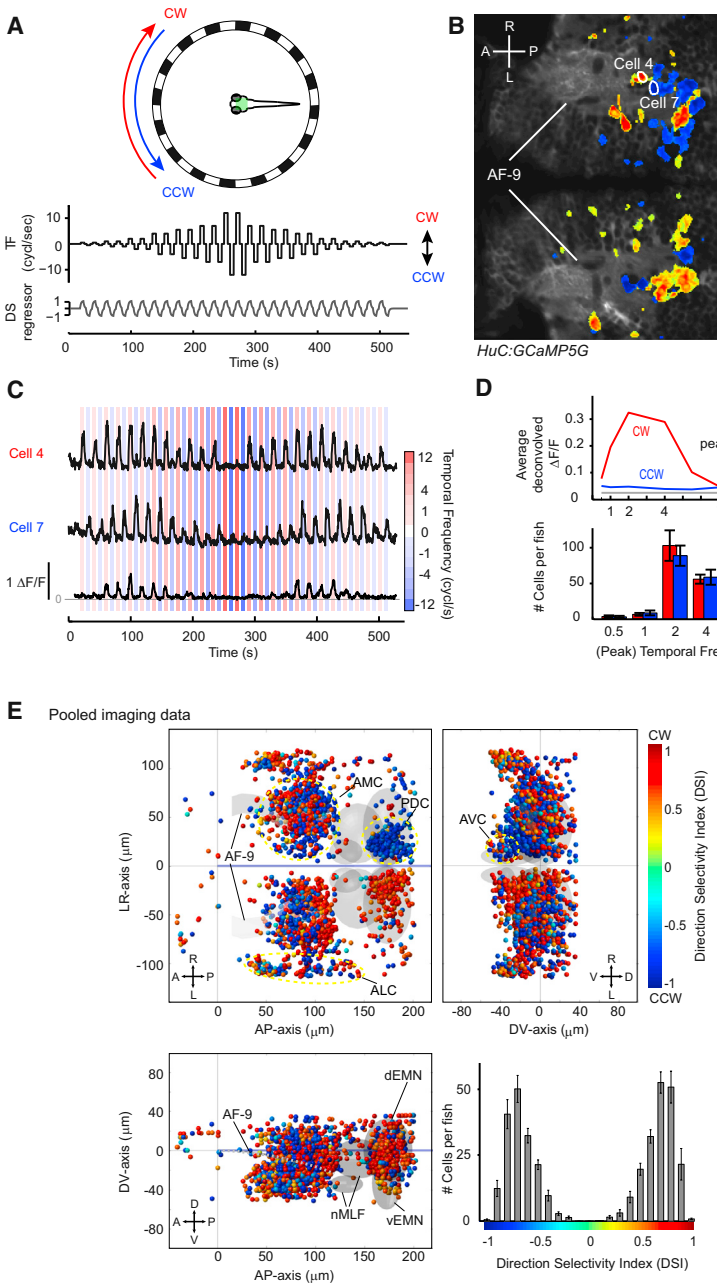

Figure 2. Calcium Imaging of the Pretectum Reveals High Degree of Direction Selectivity during Whole-Field Motion

(A) Illustration of the stimulus protocol for two-photon calcium imaging during simultaneous visual stimulation. (Top) An LED arena surrounding the fish was used for visual stimulation. The green box shows the approximate region imaged in (B). (Middle) Stimulus directions were alternated (CW or CCW) and had varying temporal frequencies (TF, 0.5–12 cycles/s). (Bottom) A direction-selective (DS) regressor was built from the stimulus protocol.

(B) 2D map of image pixels that are correlated with the DS regressor, superimposed on an optical section of the *HuC:GCaMP5G* transgenic animal. Pseudocolor scale shows the local correlation to the DS regressor (Z score, see Experimental Procedures for details). A: anterior; P: posterior; R: right; L: left.

(C) Fluorescence (ΔF/F) traces during the visual stimulus presentation. The cell numbers correspond to the ones in (B). Cell 4 responded during CW rotation, whereas cell 7 responded during CCW rotation. Both cells responded to temporal frequencies ranging from 0.5 to 7 cycles/s and less so to 12 cycles/s.

(D) (Top) Tuning curve of the cell plotted at the bottom of (C) during the CW (red) and CCW (blue) stimulations. The gray line indicates the threshold used for DSI calculation (see Experimental Procedures). (Bottom) Histogram showing the distribution of peak temporal frequencies per fish (n = 7 fish).

(E) 3D reconstructed map of CW- and CCW-responsive cells. Each dot represents a cell and is color-coded according to its direction selectivity index (DSI). Coordinates are defined as distances relative to the anterior-dorsal edge of neuropils in the diencephalon (anterior-posterior axis and dorso-ventral axis) and midline (left-right axis). dEMN indicates dorsal extraocular motor neurons; vEMN indicates ventral extraocular motor neurons; together, dEMN and vEMN correspond to the trochlear and oculomotor nuclei; nMLF indicates nucleus of the medial longitudinal fasciculus. Cells cluster in four anatomical regions (see Results): AMC, ALC, AVC, and PDC. (Lower right) Histogram of DSIs per fish (n = 7 fish). Error bars indicate SEM. Scale bar shows 50 μm. See also Figures S1–S4.

To abolish any motion artifacts induced by eye movements, we switched to a paralyzed preparation (see Experimental Procedures). Figure 2B shows an example recording of bilateral fields below the tectum, which contain AF9. Cells with CW (positive) and CCW (negative) correlations were located in close proximity to the neuropil (Figure 2B). In a typical example, one cell preferred CW motion, whereas a neighboring cell on the same side preferred CCW motion (Figure 2C; Movie S2). Their response magnitudes were often modulated by the temporal frequencies of the visual stimulus (Figures 2C and 2D). We measured the temporal frequency tuning of all cells identified by the DS regressor (n = 2,543 from seven fish) and found that the majority of them (83%) were maximally responsive to 2 or 4 cycles/s in either CW or CCW motion (Figures 2D). To quantify the direction tuning of pretectal cells, we calculated a direction selectivity index (DSI) of the calcium responses at the temporal frequency where the tuning curve of a cell reaches its peak (peak TF). For 97% of the identified cells, the absolute DSI (|DSI|) was greater than 0.35 (Figures 2E). To exclude the possibility that the DS regressor introduces a bias in favor of isolating cells that have high |DSI| and missing cells with low |DSI|, we used another regressor as a main regressor, which had a value of +1 for both CW and CCW stimulations (motion-sensitive [MS] regressor, Figure S3). The MS regressor identified more cells with low |DSI| in

comparison to the DS regressor, as expected. However, there were still more cells with high |DSI| than cells with low |DSI|, resulting in a bimodal distribution. Our results show that the vast majority of MS cells in the pretectal area are highly direction selective.

Neurons with DS Responses Are Spatially Organized in the Pretectum

To map the positions of CW- and CCW-responsive cells, we registered each calcium imaging plane within the fish's complete brain and mapped cell positions relative to the AF9 containing neuropil (see Experimental Procedures). The dorsorostral edge of the AF9 containing neuropil was defined as the origin of the reference system. We included the following oculomotor-related nuclei as anatomical landmarks in the 3D maps: nucleus of the medial longitudinal fasciculus (nMLF), as labeled by backfilling from the spinal cord, and the oculomotor nucleus and trochlear nucleus, both as labeled in the *isl1:GFP* transgenic line (Higashijima et al., 2000) (Figures 2E and S4). In the reconstructed map, CW- and CCW-correlated cells were distributed in four mirror-symmetrical pairs of clusters, which we termed anterior medial cluster (AMC), anterior lateral cluster (ALC), anterior ventral cluster (AVC), and posterior dorsal cluster (PDC) (Figure 2E; Movies S3 and S4). The AMC covers a relatively large volume surrounding the dorsal diencephalic neuropils (anterior-posterior [AP] axis = ~40 to 140 μm caudal of the origin; left-right [LR] axis = ~0 to ± 90 μm; dorso-ventral [DV] axis = ~−50 to 50 μm), and the PDC is located ~90 μm caudal of the AMC, overlapping largely with the trochlear and oculomotor nuclei, and partially with the nMLF. The ALC and AVC occupied smaller volumes lateral and ventral to the diencephalic neuropils, respectively. The spatial distribution of the clusters was highly consistent across all fish examined, while the positions of cells within the clusters were variable (n = 7) (Figure S3G).

When all the identified cells were merged in one map, a topographic organization was evident within the AMC and ALC (Figure 2E). In the AMC, the ipsiversive responses (CW response in right AMC and CCW response in left AMC) were represented more anteriorly than the contraversive responses (Figure S3E). In the ALC, the ipsiversive populations were positioned ventrally to the contraversive ones (Figure S3F). In contrast, the PDC and the AVC consisted almost exclusively of contraversive populations. These results demonstrate that CW- and CCW-responsive cells are distributed in a spatially organized manner in the midbrain and diencephalon. While the boundaries of the pretectum are not established in larval zebrafish (Lauter et al., 2013; Puelles and Rubenstein, 2003), based on position and function of AMC, ALC, and AVC, we will collectively refer to these three clusters as APT here. The PDC appears to lie outside of the APT proper (see Discussion).

Neuronal Responses Match Simple Combinations of Eye-Specific, Direction-Selective Response Properties

While rotational motion (CW or CCW) elicited strong responses in many neurons, it was unclear whether individual cells were monocularly driven (i.e., only responding to the stimulation of one eye) or binocularly driven (i.e., responding to the stimulation of both eyes). Furthermore, in the above protocol, no distinction could be made between responses to rotation and translation. We therefore designed a stimulus protocol that consisted of eight motion phases to test the complete horizontal motion repertoire. Moving gratings were first presented to only one eye at a time in either nasalward (N) or temporalward (T) direction, and then both eyes were stimulated with rotational (CW and CCW) and translational (forward [FW] and backward [BW]) motions at a temporal frequency of 4 cycles/s (Figures 3A and 3B). In order to detect cells that were active during any of the eight stimulus phases, we used a regressor in our analysis that was ON during motion stimulation and OFF during motionless stimulation (Figures 3C and 3D).

In a typical recording, calcium traces of identified cells showed diverse, but consistent, response patterns depending on the stimulated eye(s) and the direction of motion (Figure 3D). Most cells were selectively responsive to a subset of the eight stimulus phases and nonresponsive to others. This observation prompted us to systematically classify cells based on their different combinations of responses to the eight stimulus phases: we designed a panel of regressors, which represents all possible (All-or-None) combinations of the eight stimulus phases. This resulted in 2^8 = 256 regressors (Figure 4A). We then performed correlation analysis for each cell against all 256 regressors and determined the regressor that the cell is most correlated with (referred to as "best regressor"). Cells were subsequently classified by the identity of their best regressor (see Experimental Procedures).

Cells generally show high correlation coefficients between their calcium responses and best regressor (i.e., the median correlation coefficient of all cells is 0.715, ranging from 0.297 to 0.952) (Figure S6). The distribution of cells classified by the best regressor (response type) was highly nonrandom and displayed distinct peaks (n = 3,015 cells, six fish) (Figure 4A), suggesting that the pretectal area is geared toward particular computations. Sorting response types by their abundance (Figure 4B) showed that only a small fraction of possible combinations are frequently observed in the pretectum. Almost half of the response types are represented by no, or very few, cells (equal to or less than one cell per fish for about 120 response types).

A Limited Number of Logical Operations Account for a Rich Repertoire of Response Types

We reasoned that the response types described by the 256 regressors can be explained by combinational logic. Analogous to digital electronics, simple logical operators might be employed to construct a particular output from the retinal inputs. The inputs are the four basic motion stimuli (nasalward motion in the left eye [NL], temporalward motion in the left eye [TL], nasalward motion in the right eye [NR], and temporalward motion in the right eye [TR]), and the basic logical operators are AND (∧), OR (∨), and NOT (¬). The neuronal response to any monocular or binocular motion stimuli can then be described as the output from a set of logical operations. For example, a response to the nasalward motion in the left eye (NL/−), as well as to the CW and FW phases, can simply be explained

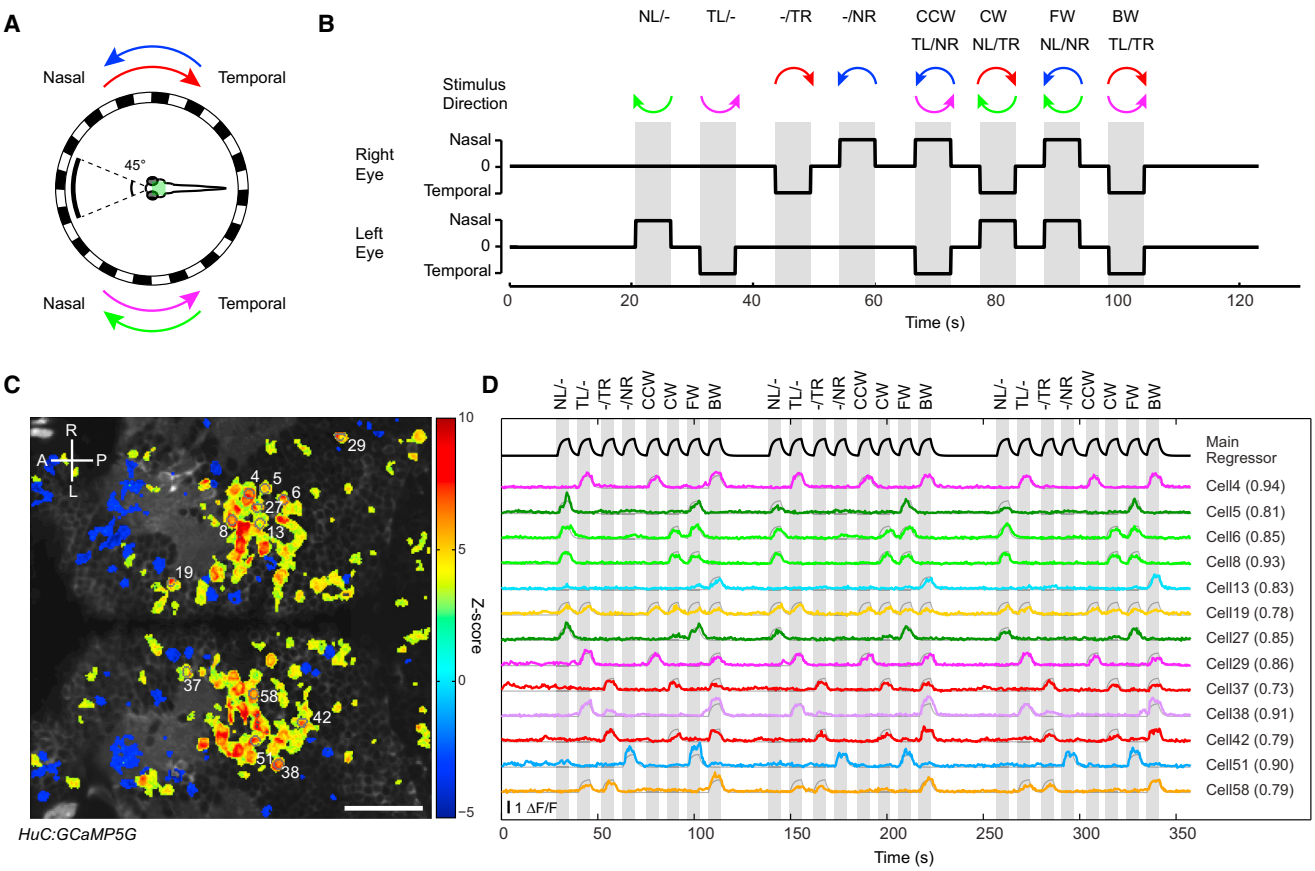

Figure 3. Calcium Imaging of *HuC:GCaMP5G* Fish in Response to Monocular and Binocular Stimulation

(A) Schematic diagram of the experimental setup. The fish's central visual field (45°) was masked to avoid stimulation of the binocular visual field. The green box shows the approximate region imaged in (C). Each half of the LED arena was rotated in nasalward (N) or temporalward (T) direction.

(B) Visual stimulation protocol. NL/– indicates nasalward motion to left eye; TL/– indicates temporalward motion to left eye; –/TR indicates temporalward motion to right eye; –/NR indicates nasalward motion to right eye; CCW indicates counter-clockwise; CW indicates clockwise; FW indicates forward; BW indicates backward.

(C) Z score map of an example recording showing motion-correlated pixels colored in red/yellow. The main regressor used for analysis is shown in the top row of (D). A indicates anterior; P indicates posterior; R indicates right; L indicates left.

(D) Example fluorescence (ΔF/F) traces (colored lines) from the single recording in (C). The eight different stimulus phases (shown in gray vertical bars) were repeated three times in one recording. Cell numbers correspond to the labels in (C). The best-performing regressor traces (gray lines, see Results) are overlaid on ΔF/F traces. Correlation coefficients with the corresponding regressors are given in parentheses. Scale bar shows 50 μm.

by NL input (Figure 4C). Likewise, a response type that is active during the NL/– and FW phases can be explained by an AND operation of NL and negated TR, described in Boolean logical operations as (NL ∧ ¬TR) (Figure 4C). This digital logic analysis allowed us to estimate the degree of complexity of the response types by determining the minimal number of logical operations that are required to construct the observed responses.

Using the Quine and McCluskey algorithm to minimize Boolean functions (see Experimental Procedures), we found that the 256 theoretically possible response types require between zero and 19 logical operations (Figure 4D; Table S1). We then quantified the number of cells according to the number of logical operations required to create the response type. The vast majority of identified cells (93%) required zero to five logical operations (Figure 4E). These results suggest that the horizontal optic flow response profile of almost every pretectal cell can be accounted for by a handful of logical operations.

The APT Predominantly Contains Monocular DS Cells and Cells that Distinguish between Rotation and Translation

The 256-regressor analysis yielded a systematic classification of diverse response types. We next decided to further categorize and name response types according to their functional implications (Figure 5A; Table 1). The "simple" category includes response types that do not require any NOT logical operators: (1) monocular DS cells, consisting of four response types that respond to either nasalward or temporalward motion presented to either left or right eye; (2) binocular DS cells, receiving information from both eyes but preferring one direction over the other; and (3) non-DS, MS cells (see

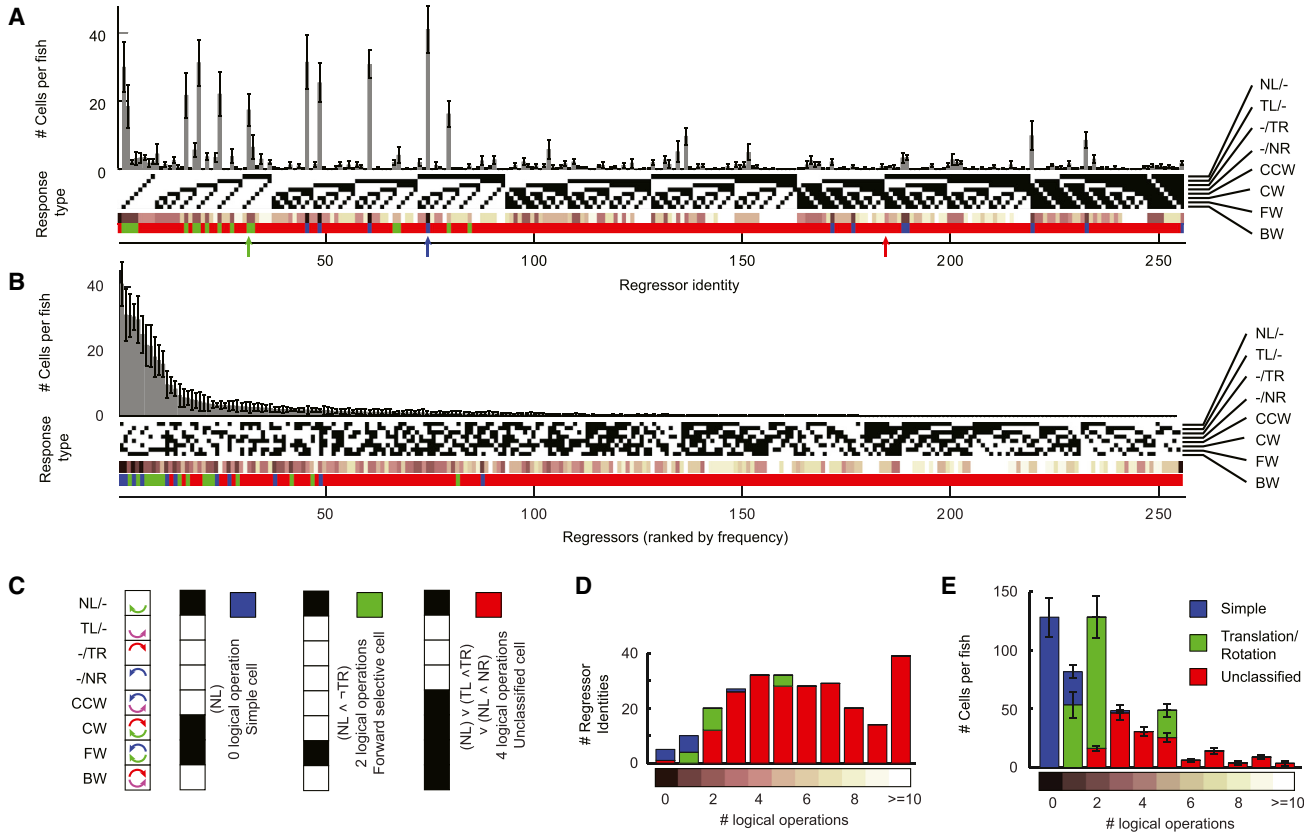

Figure 4. Distribution of Neuronal Response Types and Computational Complexity

(A) A histogram showing the number of cells per fish classified according to the 256 possible response types. The white-and-black plot below the histogram illustrates the response profile of each regressor identity/response type. Each vertical 1 × 8 line represents one response profile, and the squares indicate whether the response type is active (black) or inactive (white) during the stimulus phases indicated on the right. The copper-colored line shows the computational complexity of the response type, as in (D).

(B) The histogram from (A) sorted by abundance of the response type.

(C) Three examples, illustrating the combinational logic of response types. (Left) This type responds to NL/−, CW, and FW stimulations and thus is active whenever the left eye is stimulated nasalward. (Middle) This type responds to NL/− and FW stimulation; therefore, it is activated by NL and suppressed by TR, requiring two logical operations (AND (∧) and NOT (¬)). (Right) This type responds to NL/− and all binocular stimulations; four logical operations are needed to generate this response profile. ∧ indicates AND; ∨ indicates OR; ¬ indicates NOT.

(D) Quantification of regressor complexity. The 256 possible response types are binned according to the number of logical operations needed.

(E) Histogram of the number of cells per fish versus the number of logical operations. The color code (blue, green, and red) in (A–D) corresponds to the one used in Figure 5A. Error bars indicate SEM. See also Figures S5 and S6 and Table S1.

Table 1 for detailed descriptions of each response group). The response properties of these cells can be explained by direct input from DS RGCs and do not require further (inhibitory) processing. Despite their computational simplicity in our experimental paradigm, these cells might be more intricate regarding other properties (e.g., receptive field size). In the simple response category, the binocular DS group was much less represented than the monocular DS group, indicating that most simple cells receive input from just one eye. Also, the monocular DS group was larger than the non-DS group, consistent with our results showing that most cells are directionally tuned (see Figure 2E).

The second category consists of four groups that show dedicated responses to one of the four binocular stimulation phases (FW, BW, CW, and CCW) and therefore are selectively responsive to either translation or rotation. Twelve out of the sixteen translation-/rotation-selective response types respond to monocular stimulations but do not respond to one or more of the binocular stimulations even though they would be expected to do so based on their monocular response profiles (Figures 5A and 5B). For example, FEL cells respond to NL/− and FW, but not to CW, stimulations even though the left eye receives nasalward motion during the CW stimulation, suggesting that during the CW stimulation the response of this neuron type is suppressed by the temporalward signal received by the right eye (Figures 4C and 5A). Four out of the sixteen translation-/rotation-selective response types respond exclusively to one of the four binocular phases (FSP, BSP, CSP, and CCSP). Remarkably, we found that translation-selective cells (FW and BW) were almost as abundant as simple DS cells. In contrast, there were

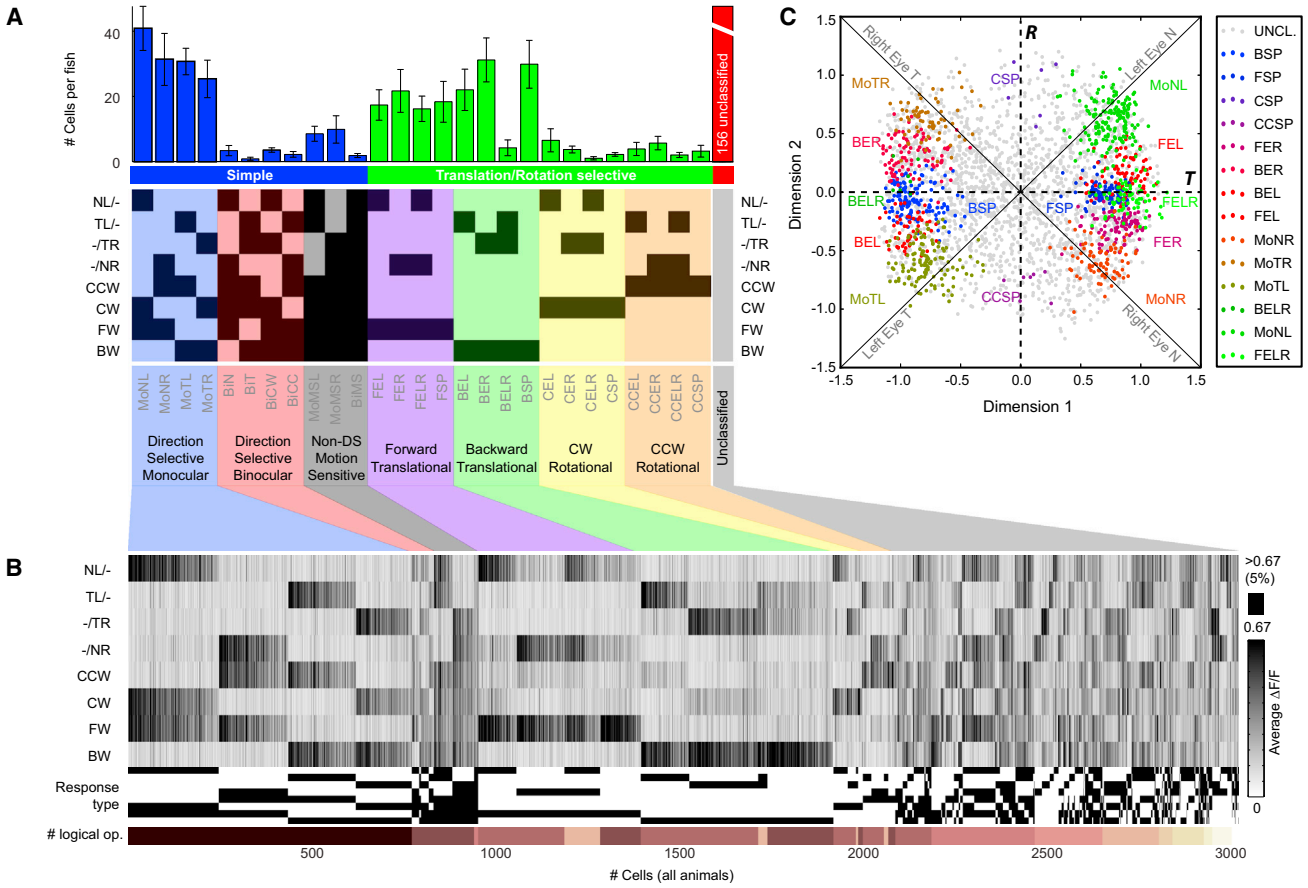

Figure 5. Frequency and Response Profiles of Functional Neuron Types

(A) Classification of 27 out of the 256 response types according to their proposed function (see Table 1). (Top) A histogram of the 27 classified response types ("simple," blue, "translation/rotation-selective," green). The remaining 229 response types were not further classified ("unclassified," red). (Middle) Response profiles of the 27 types (compare Figure 4A). (Bottom) Functional classification and nomenclature. The simple DS monocular response types and the translation-selective response types (with the exception of BELR) were significantly more abundant than expected by chance according to a permutation test with shuffled data (alpha = 0.05). The median Bonferroni corrected (n = 27), two-tailed p value for these eleven neuron types was 0.00043. Note the scarcity of binocular rotation-selective responses (yellow and orange) compared to the binocular translation-selective ones (purple and green).

(B) (Top) Raster plot showing the average responses to the eight stimulus phases for all 3,015 recorded cells. Cells are ordered according to (1) the functional response type classification (first 27 response types), (2) their computational complexity (remaining 229 response types), and (3) their correlation coefficient to the corresponding regressor (within each response type). (Middle) The Boolean profile of each cell. (Bottom) The number of logical operations predicted for each response type (same copper-color legend as in Figure 4D).

(C) Representation of the responses in a 2D space by Isometric Mapping. Dots represent the individual 3,015 cells. Neurons classified as simple monocular DS and translation-selective, as well as the CSP and CCSP neuron types from the rotation-selective groups, are color-coded according to the legend on the right (see also Table 1; UNCL. indicates unclassified). Axes are correlated with properties of the visual stimulus, namely a horizontal translation-selective and a vertical rotation-selective axis (T and R) and diagonal axes that correspond to individual eyes and motion directions. Error bars indicate SEM. See also Figures S1, S7, and S8.

substantially fewer rotation-selective cells (CW and CCW) (Figure 5A).

The remaining response types were collectively grouped as "unclassified" (31%, 156 cells per fish, and 0.7 cells per response type and fish on average). Figure 5B shows a raster plot of the identified cells from our recordings (n = 3,015 cells; six fish) ordered according to the 27 classified response types and according to response type complexity for the remaining response types. The raster plot shows that response patterns are very distinct from each other and that the absolute response magnitudes are similar within and between different response groups.

Isometric Mapping of the Responses Highlights Separated but Overlapping Distributions of Distinct Response Types

We next asked to what extent our assigned response types represent discrete or continuous processing channels. To better evaluate the quality of our classification, we applied a dimensionality reduction approach based on the Isometric Mapping algorithm (Tenenbaum et al., 2000). We remapped the eight-dimensional (8D) space, where responses are represented by 8D vectors corresponding to the average ΔF/F values during the eight stimulus phases (Figure S7), into a 2D embedding

Table 1. Summary of Response Types and Nomenclature

	Functional neuron type	Digital logic response profile (Boolean function)	# Logical operations	Proposed mechanism	Number of cells per fish ± SEM		Location in the brain	Laterality index	Active stimulus phases
Simple									NL/- TL/- -/TR -/NR CCW CW FW BW
Direction selective									
Monocular									
	MoNL	NL	0	DS RGC relay	41	± 6.8	AMC, ALC, AVC, PDC	-0.29	
	MoNR	NR	0	DS RGC relay	31	± 8.0	AMC, ALC, AVC	0.14	
	MoTL	TL	0	DS RGC relay	31	± 4.1	AMC, ALC, PDC	-0.91	
	MoTR	TR	0	DS RGC relay	25	± 5.8	AMC, ALC	0.92	
Binocular									
	BiN	NL ∨ NR	1	Binocular DS RGC input	3	± 1.6	AMC	-0.47	
	BiT	TL ∨ TR	1	Binocular DS RGC input	1	± 0.5	Sparse and scattered	1.00	
	BiCW	NL ∨ TR	1	Binocular DS RGC input	4	± 0.7	AMC	1.00	
	BiCC	TL ∨ NR	1	Binocular DS RGC input	2	± 0.9	AMC	-0.85	
Motion Sensitive									
Monocular									
	MoMSL	NL ∨ TL	1	Binocular DS RGC input	9	± 2.3	Anterior AMC, ALC	-0.92	
	MoMSR	TR ∨ NR	1	Binocular DS RGC input	10	± 4.2	Anterior AMC, ALC	0.84	
Binocular									
	BiMS	NL ∨ TL ∨ TR ∨ NR	3	Binocular DS RGC input	2	± 0.6	Sparse and scattered	0.14	
Translation selective									
Direction selective									
Forward Translation									
	FEL	NL ∧ ¬ TR	2	Inhibited by MoTR	17	± 4.6	Posterior AMC	-0.41	
	FER	NR ∧ ¬TL	2	Inhibited by MoTL	22	± 6.6	Posterior AMC, PDC	0.14	
	FELR	(NL ∧ ¬TR) ∨ (NR ∧ ¬TL)	5	Inhibited by MoTR and MoTL	16	± 3.9	Posterior AMC, PDC	-0.25	
	FSP	NR ∧ NL	1	Summated/Thresholded	18	± 6.3	Posterior AMC	0.16	
Backward Translation									
	BEL	TL ∧ ¬NR	2	Inhibited by MoNR	22	± 6.3	Anterior AMC, PDC	-0.63	
	BER	TR ∧ ¬NL	2	Inhibited by MoNL	31	± 6.7	Anterior AMC, ALC, PDC	0.64	
	BELR	(TL ∧ ¬NR) ∨ (TR ∧ ¬NL)	5	Inhibited by MoNR and MoNL	4	± 2.4	AMC	-0.08	
	BSP	TR ∧ TL	1	Summated/Thresholded	30	± 7.3	AMC, AVC	0.03	
Rotation selective									
Direction selective									
CW Rotation									
	CEL	NL ∧ ¬NR	2	Inhibited by MoNR	7	± 3.5	AMC, PDC	-0.05	
	CER	TR ∧ ¬TL	2	Inhibited by MoTL	4	± 1.1	AMC	0.76	
	CELR	(NL ∧ ¬NR) ∨ (TR ∧ ¬TL)	5	Inhibited by MoNR and MoTL	1	± 0.5	Sparse and scattered	-0.20	
	CSP	TR ∧ NL	1	Summated/Thresholded	2	± 0.5	Sparse and scattered	0.71	
CCW Rotation									
	CCEL	TL ∧ ¬TR	2	Inhibited by MoTR	4	± 2.0	AMC	-0.88	
	CCER	NR ∧ ¬NL	2	Inhibited by MoNL	6	± 2.1	AMC, PDC	0.47	
	CCELR	(TL ∧ ¬TR) ∨ (NR ∧ ¬NL)	5	Inhibited by MoTR and MoNL	2	± 0.8	Sparse and scattered	-0.33	
	CCSP	NR ∧ TL	1	Summated/Thresholded	3	± 1.8	Sparse and scattered	-0.60	
Unclassified neuron types									NL/- TL/- -/TR -/NR CCW CW FW BW
	228 response types			(mainly complex combinations)	156	± 15.8	N.D.	-0.03	

Functional neuron types: Mo: Monocular, Bi: Binocular, MS: Motion Sensitive, N: Nasalward, T: Temporalward, E: Excited by, L: Left Eye, R: Right Eye, F: Forward translation, B: Backward translation, C: Clockwise rotation, CC: Counterclockwise rotation, SP: Specific.
Digital logic gates: ¬: NOT, ∧: AND, ∨: OR.
Stimulations: NL: Nasalward motion in left eye, NR: Nasalward motion in right eye, TL: Temporalward motion in left eye, TR: Temporalward motion in right eye.
Location in the brain: AMC, anterior medial cluster; ALC, anterior lateral cluster; AVC, anterior ventral cluster; PDC, posterior dorsal cluster. Clusters were determined to be present if they were populated by more than 6 cells (for AMC and PDC) or 3 cells (for AVC and ALC) in either hemisphere. N.D.: not determined.
Laterality index: for cells in AMC only, 1: left hemisphere, −1: right hemisphere.

space (Figure 5C). Most of the frequent response types classified by the 256-regressor analysis appear well separated from each other, supporting the conclusion that our response type classification is, in principle, justified (Figure 5C). Furthermore, different response types are remapped in the embedding space with the two axes corresponding to the BW-FW direction and the CCW-CW direction (Figures 5C and S8A), with responses more concentrated along the BW-FW axis than the CCW-CW axis (Figure S8B). In order to quantify the pair-wise overlap between response types, we fitted 2D Gaussians to the distribution of each response type in the embedding space (Figure S8C) and computed a pair-wise overlap matrix (Figure S8D). Most of the response type pairs (84%) are clearly separated from each other with less than 5% overlap. Some of the neighboring pairs within the FW-selective group showed a certain degree of overlap (26% ± 29%, mean ±SD; for the BW-selective group: 28% ± 29%), revealing that the response profiles for these neuron types tend to be less distinct from each other.

To further analyze the degree of separation between response types, we tested whether distributions of a given pair of response types are better described by one-component (i.e., unimodal) or two-component (i.e., bimodal) Gaussian models based on the Akaike information criterion (Freeman and Dale, 2013) (Figure S8E). Although the FELR+FER and FELR+FEL joint distributions are more conveniently described as unimodal rather than bimodal, for all the other pairs, the joint distributions were better described with bimodal Gaussian mixture models, indicating that these pairs are well separated from each other. Taken together,

the 256-regressor analysis and the Isometric Mapping analysis show that a relatively small number of the 256 possible computations are implemented in the APT and that our response types, for the most part, correspond to discrete processing channels.

Translation-Selective Cell Classes Are Enriched in Restricted Regions of the APT

Since RGC projections are completely crossed in fish, we expected that the simple monocular DS cells that respond to left eye visual stimulation (nasalward motion in left eye [MoNL] and temporalward motion in left eye [MoTL], Figure 5A; Table 1) would reside in the right brain hemisphere and ones that respond to right eye stimulation in the left brain hemisphere, if the cells were directly postsynaptic to RGCs. Indeed, the majority of monocular DS cells with responsiveness to MoTL were found on the right side (Figure 6A; Table 1, laterality index = −0.91). However, cells with responsiveness to the opposite direction (i.e., monocular DS cells with responsiveness to MoNL) were found not only on the right side but also on the left side (Figure 6B, laterality index = −0.29). The ipsilateral MoNL population was less numerous, more restricted in distribution than the contralateral population, and positioned posterior to the contralateral population (mean positions for contralateral population = 83.1 ± 1.4 μm versus ipsilateral population = 102.57 ± 1.1 μm along the AP axis; mean ±SEM across cells from all animals; $p < 0.0001$, t test). The same observations were made for the mirror-symmetric right eye-sensitive DS cells of MoNR and MoTR response types. In the merged map (Figure 6C), the anatomical clusters AMC, ALC, and AVC are apparent. While the AMC contains all four simple monocular DS neuron types, plus many other types (see below), the ALC and AVC are almost exclusively populated by simple monocular DS cells. In the ALC, MoNL and MoNR cells were located more ventrally than MoTL and MoTR cells, showing a gradient of direction selectivity along the DV axis (Figures S9A and S9B).

We next examined the distributions of translation-/rotation-selective cells, which exhibited more complex response profiles than the simple class. FW- and BW-selective cells were distributed in smaller bilateral regions within the AMC (Figures 6D–6F and S9). BW-selective cells were more broadly distributed than the FW-selective cells within the AMC (SD for the anterior-posterior distribution equals 12.0 μm for FW-selective and 17.4 μm for BW-selective cells), and the center of the FW-selective cells was 9 μm more lateral than that for BW-selective cells ($p < 0.0001$, t test). In contrast, the sparse CW- and CCW-selective cells were broadly distributed across the entire 3D map, except in the proximity of the PDC, where cells were more clustered (Figure S9C). Together, the 3D mapping of response types suggests that simple monocular DS cells are widely distributed across all identified anatomical clusters, and more complex response types are mostly restricted to AMC and PDC and furthermore confined to subregions within the AMC.

DISCUSSION

We localized the brain region mediating the horizontal OKR by using optogenetic manipulation and identified the pretectal area (APT) in larval zebrafish. By systematic analysis of calcium responses to an array of optic flow stimuli in the horizontal plane, we determined the functional architecture of this brain region. The vast majority of the APT neurons recorded were direction selective. Both monocular and binocular stimuli were tested; among the binocular stimuli, we used rotational and translational motion phases. Cells were classified according to their response profiles into monocular (simple) and binocular (simple, translation-selective, and rotation-selective) cells. Only a small subset (eleven major and additional less-frequent types) of the 256 possible response combinations (in the horizontal plane) was encountered, showing that the APT performs highly specific computations. Many cells combine inputs from both eyes to process and distinguish between rotational and translational whole-field motion.

Channelrhodopsin (ChR2) stimulation of the APT induced horizontal OKR-like eye movements. This effect is unlikely to be caused by direct stimulation of motor neurons controlling horizontal eye movements. The abducens nucleus can be ruled out based on its location in the hindbrain. The oculomotor nucleus, on the other hand, might reside partly within the photostimulated volume. However, the oculomotor nucleus contains motor neurons controlling only one of the two extraocular muscles that move the eyes in the horizontal plane (ipsilateral medial rectus), and unilateral activation of these motor neurons would therefore be expected to only move the ipsilateral eye in nasalward direction. In contrast, we observed conjugate eye movements in both nasalward and temporalward directions. Therefore, this indicates that the OKR-like behavior was triggered upstream of motor neurons. Halorhodopsin silencing of the APT blocked the OKR, whereas tectum inactivation had no effect on the OKR, consistent with earlier laser ablation results (Roeser and Baier, 2003).

The direction of eye movements induced by ChR2 stimulation resembled those resulting from ipsiversive optic flow, which is consistent with results reported in other vertebrate species, where the pretectum contains only ipsiversive-responsive DS cells. Unilateral electrical stimulation (Collewijn, 1975; Schiff et al., 1988) or lesion (Cazin et al., 1980; Gioanni et al., 1983; Kato et al., 1988; Precht and Strata, 1980; Schiff et al., 1990) of the pretectum affects ipsiversive slow-phase eye movements. However, as reported for other teleosts (Klar and Hoffmann, 2002; Masseck and Hoffmann, 2009a), we found both ipsiversive- and contraversive-responsive cells in each hemisphere. In turtles, there is evidence that the ipsiversive-sensitive cells are essential for the OKR, while the contraversive-sensitive cells only modulate it (Fite et al., 1979). Our optogenetic experiments suggest that the situation is similar in larval zebrafish.

Our temporal frequency tuning analysis showed that most cells maximally responded to 2 or 4 cycles/s, which corresponds to stimulus velocities of 60°/s and 120°/s, respectively. Previous studies show that the slow phase velocity of the OKR behavior peaks at a stimulus velocity of around 30°/s –50°/s in larval zebrafish (Huang et al., 2006; Qian et al., 2005). The difference could be due to different velocity tuning between physiological responses and behavior, the use of different stimulation protocols (e.g., spatial frequency or monocular versus binocular

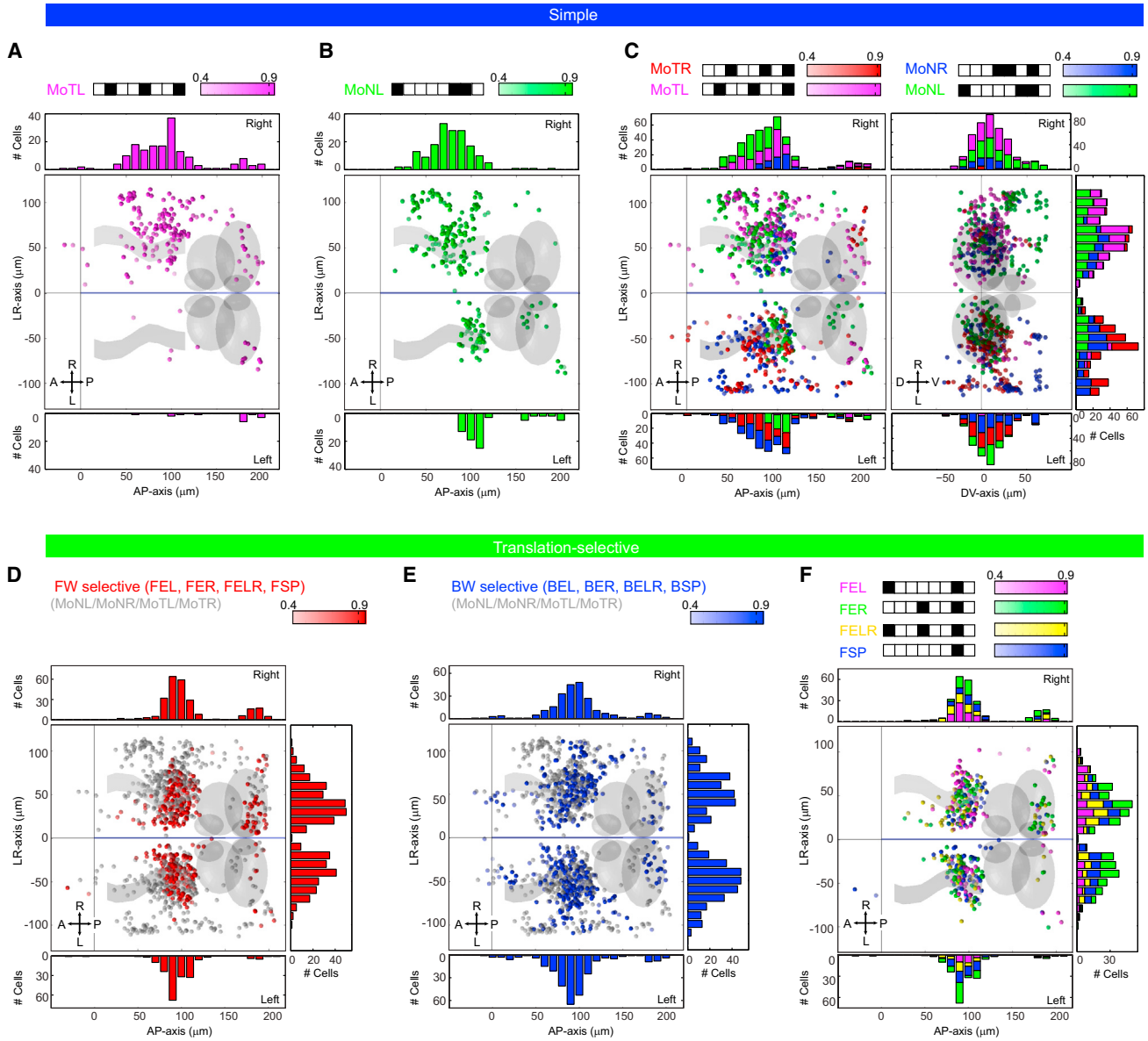

Figure 6. Spatial Organization of Simple Monocular DS Cells and Translation-Selective Cells

(A and B) Dorsal view of simple monocular DS cells reconstructed in a 3D map and responsive to temporalward motion in left eye (MoTL) (A) and nasalward motion in left eye (MoNL) (B). The Boolean profiles of the response types are shown at the top. Cell counts along the anterior-posterior (AP) axis are shown in the histograms at the top and bottom, representing right and left hemispheres, respectively.

(C) Reconstructed 3D map of all simple monocular DS neuron types. Dorsal view (left) and frontal view (right). Stacked histograms are shown corresponding to each axis.

(D and E) Dorsal views of reconstructed 3D maps of (D) forward (FW)- and (E) backward (BW)-selective groups. All four response types within the FW or BW group are pooled. All simple monocular DS cells are shown in light gray in the background.

(F) Dorsal view of the reconstructed 3D map of all neuron types within the FW-selective group. Results from six fish are pooled in all panels. In all panels, each dot represents a single cell, and its color is alpha-coded according to its correlation coefficient to the corresponding regressor (see alpha-gradient legends). Anatomical landmarks (gray) are same as in Figure 2E. See Table 1 for nomenclature. See also Figure S9. A indicates anterior; P indicates posterior; R indicates right; L indicates left; D indicates dorsal; V indicates ventral.

stimulation), or a combination of both. Further research is needed to characterize the visual response properties of individual neuron types in more detail (e.g., in order to determine their receptive field sizes and their directional tuning along the four cardinal directions) (Simpson et al., 1988; Klar and Hoffmann, 2002; Masseck and Hoffmann, 2009a; Hunter et al., 2013).

We identified four anatomical clusters that contained the majority of optic flow-responsive cells. The AMC contains the

majority of the DS cells recorded in this study and is located directly ventral to the optic tectum. We propose that the AMC corresponds to the region that previous authors referred to as "APT" (Fite, 1985; Klar and Hoffmann, 2002; Masseck and Hoffmann, 2008, 2009a). In a detailed analysis of OKR and OMR performance in zebrafish mutants affecting the retinofugal projections to different arborization fields (AFs), it was hypothesized that AF4 and/or AF9 mediate the OKR and/or OMR in larval zebrafish (Muto et al., 2005). Consistent with this hypothesis, the AMC envelops AF9, can elicit OKR-like behavior, and is largely direction selective. The ALC and AVC are separated from the AMC by a region that is only sparsely populated with DS cells; however, their response profiles (mainly simple cells) suggest that these clusters are also part of the APT. Fish possess a migrated pretectal region, known as M1, which lies ventrolateral to the tectum (Mueller and Wullimann, 2002; Ronneberger et al., 2012), in a similar position to the ALC. It is possible that the ALC corresponds to M1. The identity of the PDC is less clear, since its center is ~90 μm caudal to the center of the AMC. The PDC largely overlaps with the dorsally located extraocular motoneurons labeled in the *isl1*:*GFP* line, and to a lesser extent with the ventrally located extraocular motor neurons (vEMNs) and the nMLF. This location suggests that the PDC is involved in premotor processing and, furthermore, contains motor neurons. The PDC shows smaller ΔF/F amplitudes and has a less sharp temporal frequency tuning profile than the AMC. We suggest that the PDC is not part of the APT, but rather is downstream of it and is involved in derived premotor computations.

The logical operations each response type performs allow hypotheses concerning possible circuit connections. We assembled parsimonious wiring diagrams (Figure 7; Table 1) taking into account the frequently observed response types (≥15 cells/fish), their spatial distribution, and the assumption of a minimal number of connections and midline crossings. Although, for simplicity, we have omitted rare response types, we are aware that the abundance of cells is not a definite criterion for functional components in a circuit (i.e., rare cell types can have a critical role in circuit computation and behavior).

During rotational motion, the major active neuron types are monocular simple neurons, namely MoNL, MoTR, MoNR, and MoTL (Figures 7A, 7B, and 5A). No logical operation is required to construct their response profile, suggesting that they may receive excitatory input from DS RGCs and relay the retinal slip signal to higher-order neurons. MoNL and MoNR (but not MoTL and MoTR) are found not only on the contralateral side of the visually stimulated eye but also on the ipsilateral side. Similar results have been reported in rat (Ferrari et al., 2009). It is possible that the contralateral MoNL and MoNR cells cross the midline via a commissural pathway (posterior commissure) to innervate ipsilateral MoNL and MoNR cells, respectively. In the opossum, the absence of immunohistochemical anti-GABA staining in the commissure connecting the two NOT nuclei suggested that information from the ipsilateral eye is made available via excitatory commissural projections to ipsilateral neurons (Pereira Júnior et al., 1994; Vargas et al., 1997). In zebrafish, the connectivity might be similar, as proposed in Figures 7A and 7B. Although each brain hemisphere contains separate monocular simple cells coding for both eyes (temporalward motion signal of the contralateral eye and nasalward motion signal of the ipsilateral eye), this information is only scarcely combined in the APT to constitute rotation-selective cells (only 29 rotation-selective cells per fish, distributed over eight response types). Since the DS information from the two eyes is mostly not combined to constitute cells specifically active during rotational motion, rotational motion and rotational OKR appear to be computed largely by monocular simple cells in the APT.

In contrast, during translational motion, translation-selective cells are active in addition to the simple cells (about 160 translation-selective cells per fish) (Table 1; Figures 7C and 7D). Since these cells are suppressed during rotational stimulation, they are likely inhibited by the abundant simple cells that respond to the motion sensed by the other eye during rotation (e.g., FEL is inhibited by MoTR during CW motion) (Figures 7A and 7B). These cells integrate the information from the two eyes and apparently have binocular receptive fields, being excitatory for one eye and inhibitory for the other (except for FSP and BSP, where both eyes have an excitatory effect), and we therefore consider these cells to be "binocular." It is expected that binocular translation-selective cells are inhibited during particular monocular stimulations (e.g., FEL cells would be inhibited during the −/TR phase). However, due to the insensitivity of calcium indicators to inhibition of resting neurons, we could not detect this hypothetical inhibitory input, which could be demonstrated by intracellular electrophysiology in the future. During FW and BW motion, neural activity switches between the forward- and backward-selective networks, and these networks potentially mediate the optomotor forward swimming and turning behavior that is observed during FW and BW motion (Orger et al., 2008), respectively. The FSP cells exclusively respond to FW motion, and their response profile could be generated by combining FER and FEL with an AND operation (Figure 7C). (However, it is also possible to generate the FSP response profile by combining MoNL and MoNR with an AND operation.) The nature of the AND operation is not known: it could be achieved by thresholding, multiplying, or summating the two inputs (FER and FEL), as illustrated in Figure 7C. Alternative mechanisms are plausible (e.g., mechanisms including inhibitory, tonically active neurons, which stop firing during particular stimulus phases). Due to our use of a main regressor that is active during motion stimulation, our analysis was blind toward such tonically active cells. Using a regressor that is inactive during the motion phases, we investigated in two animals whether such tonically active cells are present (unpublished observations). While abundant light-OFF-responsive cells complicated the analysis, we only found six to seven tonically active cells per fish, suggesting that tonically active cells, which are suppressed during motion, play a minor role in the APT.

Our study reports binocularly responsive neurons within the teleostean APT. Subpopulations of neurons in the pretectum and the AOS were found to display binocular translation and rotation sensitivities in pigeons (Wylie, 2000; Wylie and Frost, 1990). In frontal-eyed mammals, binocular neurons are abundant in the NOT/DTN, established either by inputs from the cortex (Markner and Hoffmann, 1985) or by intrinsic contralateral projections within the pretectum (Ferrari et al., 2009; Pereira Júnior et al., 1994; Reber et al., 1991). The binocular neurons

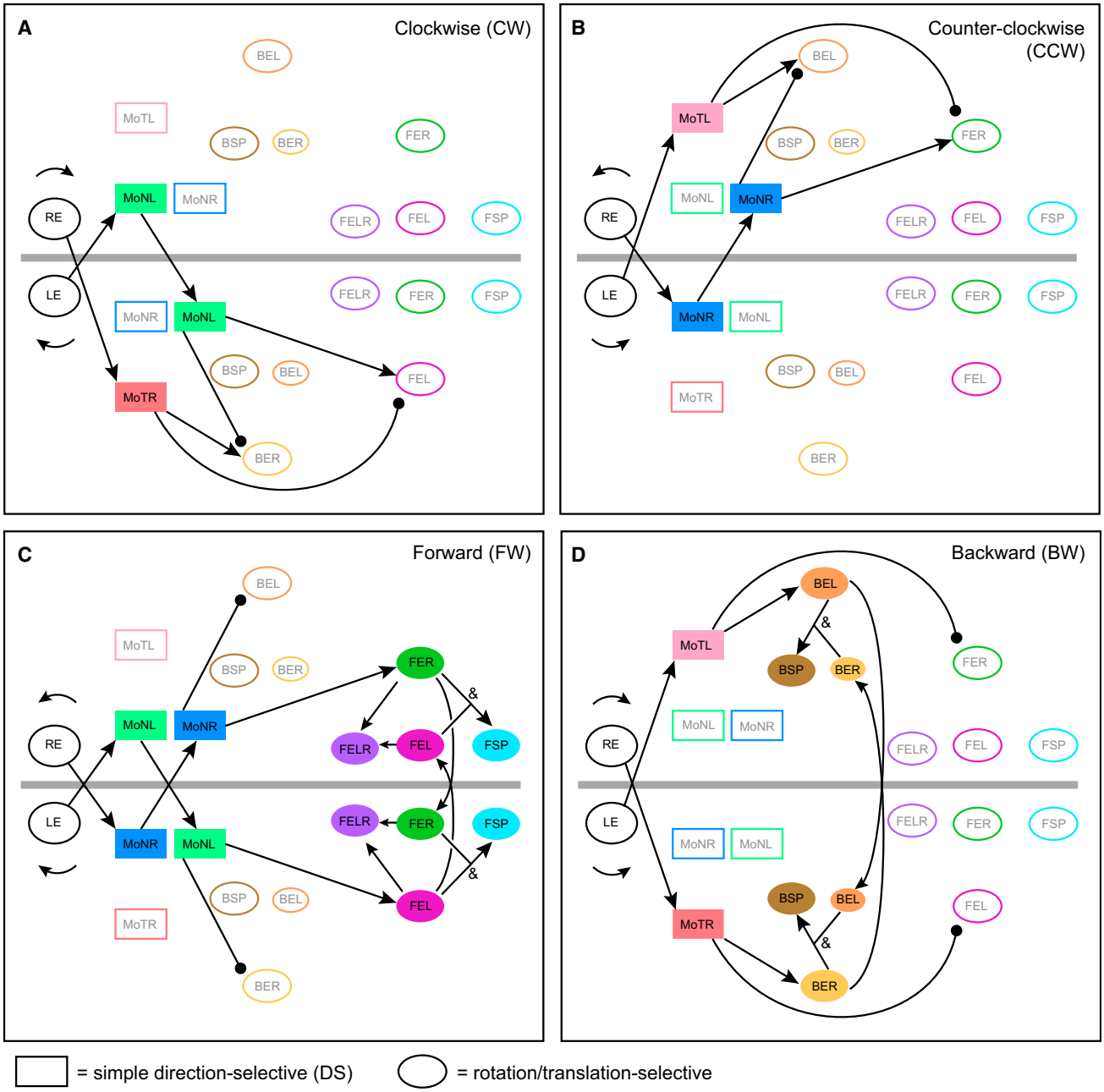

Figure 7. Proposed Circuit Model for Processing of Binocular Optic Flow in the Pretectum

(A–D) Proposed circuit model for processing (A) CW, (B) CCW, (C) FW, and (D) BW motion by the eleven most frequent functional neuron types (see Table 1). Boxes and ovals indicate simple and translation-/rotation-selective classes, respectively. Open and filled objects represent active and inactive states of cells, respectively. Arrows indicate putative excitatory and inhibitory connections.

(A) During CW motion, nasalward motion in the left eye and temporalward motion in the right eye activate MoNL and MoTR, respectively. FEL and BER, which are active during FW and BW phases but not during CW phase, are inhibited by MoTR and MoNL, respectively.

(B) During CCW motion, nasalward motion in the right eye and temporalward motion in the left eye activate MoNR and MoTL, respectively. FER and BEL, which are active during FW and BW phases but not during CCW phase, are inhibited by MoTL and MoNR, respectively.

(C) During FW motion, nasalward motion in the left and right eyes activates MoNL and MoNR, and then FEL and FER, respectively. This allows further activation of FELR, FSP, and the contralateral population of FEL and FER.

(D) During BW motion, temporalward motion in the left and right eyes activates MoTL and MoTR, and then BEL and BER, respectively. This allows further activation of BSP and contralateral population of BEL and BER. Position of neuron types reflects their laterality in the brain (see laterality index in Table 1). Gray lines denote the midline. See Table 1 for the nomenclature of the response types and Discussion for detail. LE indicates left eye; RE indicates right eye.

in the zebrafish APT are, for the most part, different from these binocular neurons in other species in that the binocular interactions are mediated by inhibitory interactions. The inhibitory nature of the binocularity in many translation-selective cells, as well as the scarcity of binocular rotation-selective cells, might have caused binocular processing to be overlooked in previous studies in fish.

Why is the degree of binocularity different between rotational and translational motion processing in the APT? We suggest that the difference in computation could be related to the fact that an animal has two eyes and one body and that translation evokes largely body movements and rotation largely eye movements. During whole-field stimulation, the two eyes can move independently to some degree in zebrafish (Qian et al., 2005; Rinner et al., 2005) as in other fish species (Fritsches and Marshall, 2002). To control movement of one eye, it is useful to retain monocular information in the APT. The yoking of both eyes during monocular stimulation, which occurs in zebrafish, would be generated further downstream (e.g., brain regions such as the cerebellum, inferior olive, the hindbrain integrator for horizontal eye movements, and vestibular or motor nuclei). In contrast, during the OMR, a single direction of swimming needs to be determined based on the combined information from both eyes in order to drive forward swimming or near-180° turning during forward and backward translational motion, respectively (Orger et al., 2008). We hypothesize that the decision to swim forward (or turn around) is made early in the APT and passed on to reticulospinal neurons that control locomotion. Although we note that rotational motion can also induce directional changes of the body involving turns, this difference in ethological demands could underlie the different degrees of binocularity between rotational and translational motion.

The digital logic approach allowed us to thoroughly analyze the multidimensional response profiles (left eye, right eye, nasalward, temporalward, monocular, and binocular) and determine the specificity of APT's responses. The APT, although considered still a sensory area, appears to be geared toward behavioral function, since a substantial population of cells (~30%) had a preference for just one particular binocular stimulus (namely, FW or BW). The specific wiring diagrams derived from our analysis provide a springboard for understanding how whole-field motion is computed within the APT at the circuit level. Future studies will identify neurotransmitter phenotypes and explore the synaptic connectivity of the identified cells.

EXPERIMENTAL PROCEDURES

All animal procedures conformed to the institutional guidelines of the Max Planck Society, the University of Freiburg, and the local governments (Regierung von Oberbayern, Regierungspräsidium Freiburg).

Optical stimulation and OKR assay were performed using the transgenic fish lines *Tg*(*UAS*:*ChR2*(*H134R*)*-mCherry*)*s1986t*; *Tg*(*UAS*:*NpHR-mCherry*)*s1989t*; *Et*(*E1b*:*Gal4-VP16*)*s1101t* as described previously (Arrenberg et al., 2009; Schoonheim et al., 2010). Calcium imaging was performed using a two-photon microscope setup based on a MOM microscope (Sutter Instruments) and the *HuC*:*GCaMP5G* (*Tg*(*elavl3*:*GCaMP5G*)*a4598*) line (Ahrens et al., 2013). Moving gratings were presented using four LED panels surrounding the animal. LEDs were only ON during the fly-back time of the scanning mirrors. For correlation analysis of calcium image time series, we used custom Matlab scripts based on Miri et al. (2011). 3D mapping of recorded cells was performed by registering the 2D recordings to a Z stack using a custom-written Matlab script. Detailed methods are available in the Supplemental Experimental Procedures.

SUPPLEMENTAL INFORMATION

Supplemental Information includes nine figures, one table, five movies, and Supplemental Experimental Procedures and can be found with this article online at http://dx.doi.org/10.1016/j.neuron.2014.02.043.

ACKNOWLEDGMENTS

We thank Jennifer Li, Drew Robson, Michael Orger, and Alexander Schier for sharing their *HuC*:*GCaMP5G* line before publication. We thank Sebastian Reinig for help with the deconvolution algorithm. We thank Tod Thiele, Estuardo Robles, António M. Fernandes, and members of our laboratories for discussions. Support was provided by the Max Planck Society (F.K., M.D.M., and H.B.), the Center for Integrative Protein Science Munich (H.B. and M.D.M.), the Toyobo Biofoundation (F.K.), a Human Frontier Science Program fellowship (F.K.), and the Deutsche Forschungsgemeinschaft (DFG EXC294 BIOSS, SFB780 B6, and INST 39/815-1 to W.D.).

Accepted: February 18, 2014
Published: March 19, 2014

REFERENCES

Ahrens, M.B., Orger, M.B., Robson, D.N., Li, J.M., and Keller, P.J. (2013). Whole-brain functional imaging at cellular resolution using light-sheet microscopy. Nat. Methods *10*, 413–420.

Akerboom, J., Chen, T.-W., Wardill, T.J., Tian, L., Marvin, J.S., Mutlu, S., Calderón, N.C., Esposti, F., Borghuis, B.G., Sun, X.R., et al. (2012). Optimization of a GCaMP calcium indicator for neural activity imaging. J. Neurosci. *32*, 13819–13840.

Arrenberg, A.B., Del Bene, F., and Baier, H. (2009). Optical control of zebrafish behavior with halorhodopsin. Proc. Natl. Acad. Sci. USA *106*, 17968–17973.

Baier, H., and Scott, E.K. (2009). Genetic and optical targeting of neural circuits and behavior—zebrafish in the spotlight. Curr. Opin. Neurobiol. *19*, 553–560.

Barlow, H.B., and Hill, R.M. (1963). Selective sensitivity to direction of movement in ganglion cells of the rabbit retina. Science *139*, 412–414.

Brockerhoff, S.E., Hurley, J.B., Janssen-Bienhold, U., Neuhauss, S.C., Driever, W., and Dowling, J.E. (1995). A behavioral screen for isolating zebrafish mutants with visual system defects. Proc. Natl. Acad. Sci. USA *92*, 10545–10549.

Burrill, J.D., and Easter, S.S., Jr. (1994). Development of the retinofugal projections in the embryonic and larval zebrafish (*Brachydanio rerio*). J. Comp. Neurol. *346*, 583–600.

Cazin, L., Precht, W., and Lannou, J. (1980). Pathways mediating optokinetic responses of vestibular nucleus neurons in the rat. Pflugers Arch. *384*, 19–29.

Collewijn, H. (1975). Oculomotor areas in the rabbits midbrain and pretectum. J. Neurobiol. *6*, 3–22.

Del Bene, F., and Wyart, C. (2012). Optogenetics: a new enlightenment age for zebrafish neurobiology. Dev. Neurobiol. *72*, 404–414.

Euler, T., Hausselt, S.E., Margolis, D.J., Breuninger, T., Castell, X., Detwiler, P.B., and Denk, W. (2009). Eyecup scope–optical recordings of light stimulus-evoked fluorescence signals in the retina. Pflüg. Arch. *457*, 1393–1414.

Ferrari, R., Fonda, S., Corradini, M., and Biral, G. (2009). The commissural transfer of the horizontal optokinetic signal in the rat: a c-Fos study. Exp. Brain Res. *198*, 85–94.

Fite, K.V. (1985). Pretectal and accessory-optic visual nuclei of fish, amphibia and reptiles: theme and variations. Brain Behav. Evol. *26*, 71–90.

Fite, K.V., Reiner, A., and Hunt, S.P. (1979). Optokinetic nystagmus and the accessory optic system of pigeon and turtle. Brain Behav. Evol. *16*, 192–202.

Freeman, J.B., and Dale, R. (2013). Assessing bimodality to detect the presence of a dual cognitive process. Behav. Res. Methods *45*, 83–97.

Fritsches, K.A., and Marshall, N.J. (2002). Independent and conjugate eye movements during optokinesis in teleost fish. J. Exp. Biol. *205*, 1241–1252.

Gioanni, H., Rey, J., Villalobos, J., Richard, D., and Dalbera, A. (1983). Optokinetic nystagmus in the pigeon (Columba livia). II. Role of the pretectal nucleus of the accessory optic system (AOS). Exp. Brain Res. *50*, 237–247.

Higashijima, S., Hotta, Y., and Okamoto, H. (2000). Visualization of cranial motor neurons in live transgenic zebrafish expressing green fluorescent protein under the control of the islet-1 promoter/enhancer. J. Neurosci. *20*, 206–218.

Huang, Y.-Y., and Neuhauss, S.C.F. (2008). The optokinetic response in zebrafish and its applications. Front. Biosci. *13*, 1899–1916.

Huang, Y.-Y., Rinner, O., Hedinger, P., Liu, S.-C., and Neuhauss, S.C.F. (2006). Oculomotor instabilities in zebrafish mutant belladonna: a behavioral model for congenital nystagmus caused by axonal misrouting. J. Neurosci. *26*, 9873–9880.

Hunter, P.R., Lowe, A.S., Thompson, I.D., and Meyer, M.P. (2013). Emergent properties of the optic tectum revealed by population analysis of direction and orientation selectivity. J. Neurosci. *33*, 13940–13945.

Karten, J.H., Fite, K.V., and Brecha, N. (1977). Specific projection of displaced retinal ganglion cells upon the accessory optic system in the pigeon (Columbia livia). Proc. Natl. Acad. Sci. USA *74*, 1753–1756.

Kato, I., Harada, K., Hasegawa, T., and Ikarashi, T. (1988). Role of the nucleus of the optic tract of monkeys in optokinetic nystagmus and optokinetic after-nystagmus. Brain Res. *474*, 16–26.

Klar, M., and Hoffmann, K.-P. (2002). Visual direction-selective neurons in the pretectum of the rainbow trout. Brain Res. Bull. *57*, 431–433.

Lauter, G., Söll, I., and Hauptmann, G. (2013). Molecular characterization of prosomeric and intraprosomeric subdivisions of the embryonic zebrafish diencephalon. J. Comp. Neurol. *521*, 1093–1118.

Markner, C., and Hoffmann, K.P. (1985). Variability in the effects of monocular deprivation on the optokinetic reflex of the non-deprived eye in the cat. Exp. Brain Res. *61*, 117–127.

Masseck, O.A., and Hoffmann, K.-P. (2008). Responses to moving visual stimuli in pretectal neurons of the small-spotted dogfish (*Scyliorhinus canicula*). J. Neurophysiol. *99*, 200–207.

Masseck, O.A., and Hoffmann, K.-P. (2009a). Question of reference frames: visual direction-selective neurons in the accessory optic system of goldfish. J. Neurophysiol. *102*, 2781–2789.

Masseck, O.A., and Hoffmann, K.-P. (2009b). Comparative neurobiology of the optokinetic reflex. Ann. N Y Acad. Sci. *1164*, 430–439.

McLean, D.L., and Fetcho, J.R. (2011). Movement, technology and discovery in the zebrafish. Curr. Opin. Neurobiol. *21*, 110–115.

Miri, A., Daie, K., Burdine, R.D., Aksay, E., and Tank, D.W. (2011). Regression-based identification of behavior-encoding neurons during large-scale optical imaging of neural activity at cellular resolution. J. Neurophysiol. *105*, 964–980.

Montgomery, N., Fite, K.V., and Bengston, L. (1981). The accessory optic system of Rana pipiens: neuroanatomical connections and intrinsic organization. J. Comp. Neurol. *203*, 595–612.

Mueller, T., and Wullimann, M.F. (2002). BrdU-, neuroD (nrd)- and Hu-studies reveal unusual non-ventricular neurogenesis in the postembryonic zebrafish forebrain. Mech. Dev. *117*, 123–135.

Muto, A., Orger, M.B., Wehman, A.M., Smear, M.C., Kay, J.N., Page-McCaw, P.S., Gahtan, E., Xiao, T., Nevin, L.M., Gosse, N.J., et al. (2005). Forward genetic analysis of visual behavior in zebrafish. PLoS Genet. *1*, e66.

Neuhauss, S.C.F., Biehlmaier, O., Seeliger, M.W., Das, T., Kohler, K., Harris, W.A., and Baier, H. (1999). Genetic disorders of vision revealed by a behavioral screen of 400 essential loci in zebrafish. J. Neurosci. *19*, 8603–8615.

Nikolaou, N., Lowe, A.S., Walker, A.S., Abbas, F., Hunter, P.R., Thompson, I.D., and Meyer, M.P. (2012). Parametric functional maps of visual inputs to the tectum. Neuron *76*, 317–324.

Orger, M.B., Smear, M.C., Anstis, S.M., and Baier, H. (2000). Perception of Fourier and non-Fourier motion by larval zebrafish. Nat. Neurosci. *3*, 1128–1133.

Orger, M.B., Kampff, A.R., Severi, K.E., Bollmann, J.H., and Engert, F. (2008). Control of visually guided behavior by distinct populations of spinal projection neurons. Nat. Neurosci. *11*, 327–333.

Pereira, A., Volchan, E., Vargas, C.D., Penetra, L., and Rocha-Miranda, C.E. (2000). Cortical and subcortical influences on the nucleus of the optic tract of the opossum. Neuroscience *95*, 953–963.

Pereira Júnior, A., Volchan, E., Bernardes, R.F., and Rocha-Miranda, C.E. (1994). Binocularity in the nucleus of the optic tract of the opossum. Exp. Brain Res. *102*, 327–338.

Precht, W., and Strata, P. (1980). On the pathway mediating optokinetic responses in vestibular nuclear neurons. Neuroscience *5*, 777–787.

Puelles, L., and Rubenstein, J.L.R. (2003). Forebrain gene expression domains and the evolving prosomeric model. Trends Neurosci. *26*, 469–476.

Qian, H., Zhu, Y., Ramsey, D.J., Chappell, R.L., Dowling, J.E., and Ripps, H. (2005). Directional asymmetries in the optokinetic response of larval zebrafish (Danio rerio). Zebrafish *2*, 189–196.

Reber, A., Sarrau, J.M., Carnet, J., Magnin, M., and Stelz, T. (1991). Horizontal optokinetic nystagmus in unilaterally enucleated pigmented rats: role of the pretectal commissural fibers. J. Comp. Neurol. *313*, 604–612.

Renninger, S.L., and Orger, M.B. (2013). Two-photon imaging of neural population activity in zebrafish. Methods *62*, 255–267.

Rinner, O., Rick, J.M., and Neuhauss, S.C.F. (2005). Contrast sensitivity, spatial and temporal tuning of the larval zebrafish optokinetic response. Invest. Ophthalmol. Vis. Sci. *46*, 137–142.

Roeser, T., and Baier, H. (2003). Visuomotor behaviors in larval zebrafish after GFP-guided laser ablation of the optic tectum. J. Neurosci *23*, 3726–3734.

Ronneberger, O., Liu, K., Rath, M., Rueß, D., Mueller, T., Skibbe, H., Drayer, B., Schmidt, T., Filippi, A., Nitschke, R., et al. (2012). ViBE-Z: a framework for 3D virtual colocalization analysis in zebrafish larval brains. Nat. Methods *9*, 735–742.

Scalia, F. (1972). The termination of retinal axons in the pretectal region of mammals. J. Comp. Neurol. *145*, 223–257.

Schiff, D., Cohen, B., and Raphan, T. (1988). Nystagmus induced by stimulation of the nucleus of the optic tract in the monkey. Exp. Brain Res. *70*, 1–14.

Schiff, D., Cohen, B., Büttner-Ennever, J., and Matsuo, V. (1990). Effects of lesions of the nucleus of the optic tract on optokinetic nystagmus and after-nystagmus in the monkey. Exp. Brain Res. *79*, 225–239.

Schoonheim, P.J., Arrenberg, A.B., Del Bene, F., and Baier, H. (2010). Optogenetic localization and genetic perturbation of saccade-generating neurons in zebrafish. J. Neurosci. *30*, 7111–7120.

Simpson, J.I., Leonard, C.S., and Soodak, R.E. (1988). The accessory optic system of rabbit. II. Spatial organization of direction selectivity. J. Neurophysiol. *60*, 2055–2072.

Tenenbaum, J.B., de Silva, V., and Langford, J.C. (2000). A global geometric framework for nonlinear dimensionality reduction. Science *290*, 2319–2323.

Vanegas, H., and Ito, H. (1983). Morphological aspects of the teleostean visual system: a review. Brain Res. *287*, 117–137.

Vaney, D.I., Sivyer, B., and Taylor, W.R. (2012). Direction selectivity in the retina: symmetry and asymmetry in structure and function. Nat. Rev. Neurosci. *13*, 194–208.

Vargas, C.D., Volchan, E., Hokoç, J.N., Pereira, A., Bernardes, R.F., and Rocha-Miranda, C.E. (1997). On the functional anatomy of the nucleus of the optic tract-dorsal terminal nucleus commissural connection in the opossum (*Didelphis marsupialis aurita*). Neuroscience *76*, 313–321.

Wyart, C., and Del Bene, F. (2011). Let there be light: zebrafish neurobiology and the optogenetic revolution. Rev. Neurosci. *22*, 121–130.

Wylie, D.R. (2000). Binocular neurons in the nucleus lentiformis mesencephali in pigeons: responses to translational and rotational optic flowfields. Neurosci. Lett. *291*, 9–12.

Wylie, D.R., and Frost, B.J. (1990). Binocular neurons in the nucleus of the basal optic root (nBOR) of the pigeon are selective for either translational or rotational visual flow. Vis. Neurosci. *5*, 489–495.